Polymer Testing 104 (2021) 107404

Contents lists available at ScienceDirect

Polymer Testing

journal homepage: www.elsevier.com/locate/polytest

Strain dependent crystallization of isotactic polypropylene during solid-state stretching

Xiang Liu [a], Lin Zou [a], Baobao Chang [a,*], Honghui Shi [a], Qingqing Yang [a], Kaichang Cheng [a], Taolin Li [a], Konrad Schneider [b], Gert Heinrich [b,c], Chuntai Liu [a], Changyu Shen [a]

[a] Key Laboratory of Materials Processing and Mold, Ministry of Education; National Engineering Research Center for Advanced Polymer Processing Technology, Zhengzhou University, Zhengzhou, 450002, China
[b] Leibniz-Institut für Polymerforschung Dresden, Dresden, D-01069, Germany
[c] Institut für Textilmaschinen und Textile Hochleistungswerkstofftechnik, Technische Universität Dresden, Dresden, D-01069, Germany

ARTICLE INFO

Keywords:
Solid-state stretching
Crystallization
Wide angle X-ray scattering
Isotactic polypropylene

ABSTRACT

In this study, the crystallization behavior of oriented isotactic polypropylene during solid-state stretching was investigated by in-situ wide-angle X-ray scattering. Results showed that a new arc appeared on the (040) reflection with the previous arcs remained when the stretching direction was inclined to the initial orientation direction, as a result of stretching induced crystallization. The crystallization process occurred later than the yielding but earlier than the strain hardening. The crystallinity of the newly formed crystal showed a linear dependence on the Hencky strain, and the slope of the plot was more sensitive to the stretching angle rather than the stretching temperature. Lastly, the stress relaxation test showed that the crystallinity was linear correlated to the amorphous phase orientation. The Pearson correlation coefficient was as high as −0.99, suggesting that the crystallization process is originated from the orientation of the chain network during stretching.

1. Introduction

Since the establishment of polymer science by Staudinger in 1920 [1], this field has gained tremendous development in the last century [2,3]. Currently, various polymer materials have been synthesized artificially or found directly in nature, and playing an important role in daily life, packaging, automobile, biomedicine, national defense, aerospace, etc. [4–7]. Among all polymer materials, the semicrystalline polymer is a group of polymer that crystallizes into diverse crystal forms and morphologies during processing.

Upon appropriate drawing condition, the morphology of the semicrystalline polymer will be transferred from isotropic to highly oriented one. By making use of this transition, Coates and Ward developed a solid-phase processing method for the semicrystalline polymer to fabricate fibers, rods, and tapes with extremely high strength [8–10]. To be more specific, polypropylene (PP) rods prepared by die drawing presented a room temperature Young's modulus up to 20.6 GPa [8], Young's modulus and tensile strength of ultra-draw high density polyethylene (HDPE) were reported to be as high as 70 GPa and 1.5 GPa [9,10]. More recently, solid-phase processing can be also used to prepare HDPE films with a transmittance of ~90% [11,12].

The morphology transition during drawing is represented by the deformation of the initial structure and the formation of a new structure. The mechanism responsible for the morphology transition has been gaining massive interest [13–22]. Bowden and Young [13] proposed that the deformation of polymer crystals can be regarded as a crystallographic slip governed process, which is similar to that of metals. The slip process can be also divided into the fibrillar slip, the lamella slip, and the chain slip [14]. The crystallographic slip theory is especially suitable when describing the relationship between the yield stress and deformation rate or temperature, but focuses the interest rarely on the morphology evolution and orientation development. Peterlin [15,16] revealed that there exist three stages of deformation during the cold drawing of semicrystalline polymer, which is the plastic deformation of original spherulite, the discontinuous transformation of the spherulite into fiber by micro-necking, and lastly the plastic deformation of the fiber structure. More important, Peterlin found that the long period of the original sample hardly influences the new long period after necking [16], suggesting that a simple rotation of the original random lamellae to the oriented state is insufficient to account for the establishment of a

* Corresponding author.
E-mail address: bbchang@zzu.edu.cn (B. Chang).

https://doi.org/10.1016/j.polymertesting.2021.107404
Received 5 August 2021; Received in revised form 3 October 2021; Accepted 28 October 2021
Available online 29 October 2021
0142-9418/© 2021 The Authors. Published by Elsevier Ltd. This is an open access article under the CC BY-NC-ND license (http://creativecommons.org/licenses/by-nc-nd/4.0/).

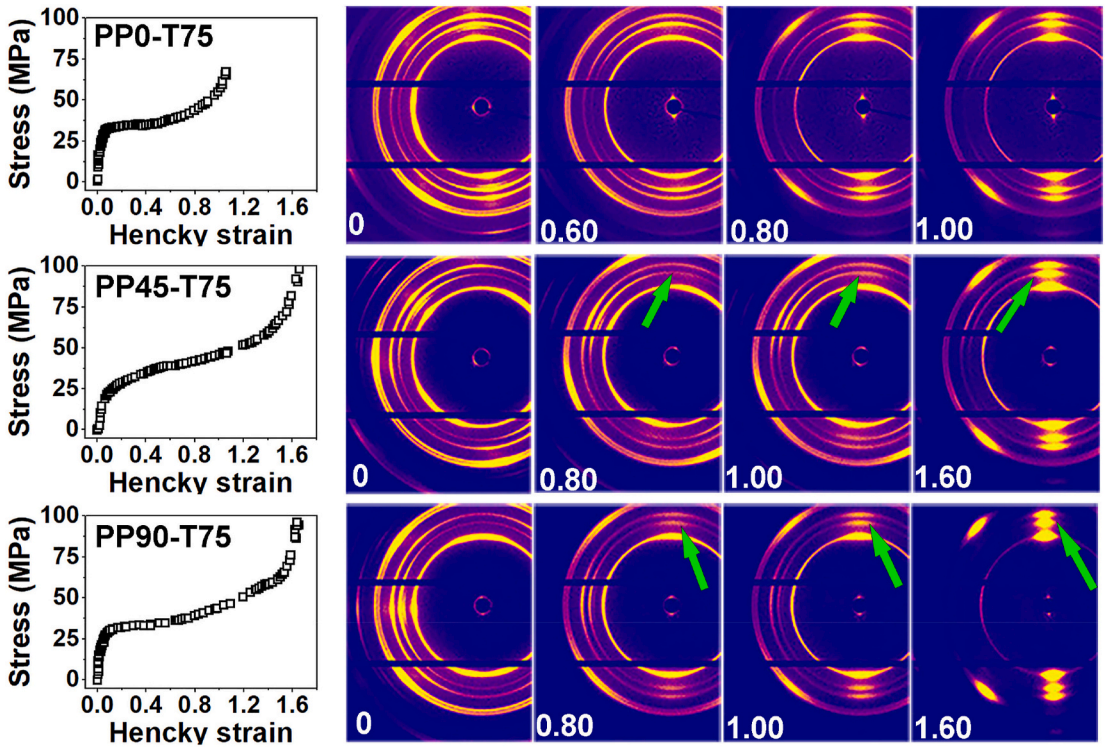

Fig. 1. Stress-strain curves of PP0-T75, PP45-T75, PP90-T75, and their corresponding representative WAXS patterns during stretching. The number marked on the corner labels the Hencky strain when the pattern was recorded. The stretching direction was horizontal.

highly oriented structure. Nowadays, a consensus is gradually reached that it is the crystallization process that dominates the formation of new structures, especially at large drawing regimes and high drawing temperature [21,23–31].

The crystallization behavior is influenced by the drawing temperature, the initial stereoregular of chains, and so on. Similar to the crystallization under static conditions, the reciprocal thickness of lamellae formed during drawing through crystallization also shows a linear dependence on the crystallization temperature, although the lamellae thickness is thinner [23–26]. The morphology of the new structure can be either rod-shaped or fibrillar structure, depending on stretch ratio, stretch speed, and annealing time [32]. For homo-iPP depending on the drawing temperature, three regions can be identified which are oriented structure with the mesophase, fibrillation with both mesophase and α-iPP, and fibrillation with complete α-iPP [29]. The mesophase phase formation at low temperatures is also verified in other reports [30]. For stereoregular iPP [31], at room temperature, the fibrillary morphology is characterized by rod-like fibrillary entities containing mesomorphic aggregates separated by amorphous regions. Instead, the morphology developed at 60 °C is made up of a fibrillary network for the more stereoregular sample and of rod-like fibrillary entities for the less stereoregular sample.

Different from the fully isotropic specimen, upon drawing the morphology transition in the partially oriented sample is affected greatly by the angle between the stretching direction and the original orientation direction [28,33–35]. For simplicity, this angle will be named as deviation angle (DA). Zhou and Wilkes [34] stretched the oriented PE specimens at DAs of 0°, 45°, and 90°. The results showed that in the initial deformation stage, lamellar separation, lamellar shear, and lamellar break-up were the dominant initial deformation mechanisms for the 0°, 45°, and 90° deformations. At larger strain, the 45° and 90° deformations generated a final microfibril morphology oriented along the stretch direction, while the 0° deformation resulted in the broken of the specimen. Whereas, Thévenon and Fulchiron [28] suggested that the reorientation in 90° deformations is most likely caused by the crystalline plane slipping. Fritz-Popovski et al. deformed the poly (ethylene terephthalate) films with oriented lamellar structure at 0°, 45°, and 90° [35]. Results showed that as DA is 90°, the finite size fragmented lamellae arrange in a chequerboard type structure.

In our previous report [33], iPP was used as a template material, and the structural evolution of partially oriented iPP deformed at small deformation with DAs of 0°, 15°, 30°, 45°, and 90° was investigated by in-situ synchrotron wide-angle X-ray scattering (WAXS) and small-angle X-ray scattering (SAXS). Results suggested that both lamellae slip and chain slip are triggered at the beginning of deformation as DA was 30° and 45°, whereas only lamellae separation or compression occur when DA was 0° or 90°. In this study, the focus will be concentrated on the crystallization behavior during stretching at a large deformation region, especially the relationship between the crystallinity and macroscopic strain. The paper is organized as follows: in the experimental section the material and the stretching set-up are described; in results and discussion the influence of DA and stretching temperature on the crystallization behavior will be illustrated; lastly, the mechanism responsible for the crystallization process will be proposed. This work attempts to providing new insight into the crystallization behavior of semi-crystalline polymer during solid-state stretching.

2. Experimental section

IPP with a brand of HD120MO was purchased from Borealis, Austria. The melt flow index is 8 g/10 min under 230 °C and 2.16 kg (ASTM D1238). The weight-average and number-average molecular weights are 365 kg/mol and 67.6 kg/mol, respectively. The specimen with waist-shape was cut from the injection-molded plate. The narrowest part of the specimen is 4 mm × 1 mm. The injection molding parameters were provided in our previous work. DA was controlled by Computerized Numerical Controlled (CNC) cutting. More information about the sample preparation can be found Fig. S1 in the Supporting Information. For simplification, the specimens were labeled as PP*x*-T*y* with *x* labels DA and *y* labels the stretching temperature. For example, PP45-T75 means

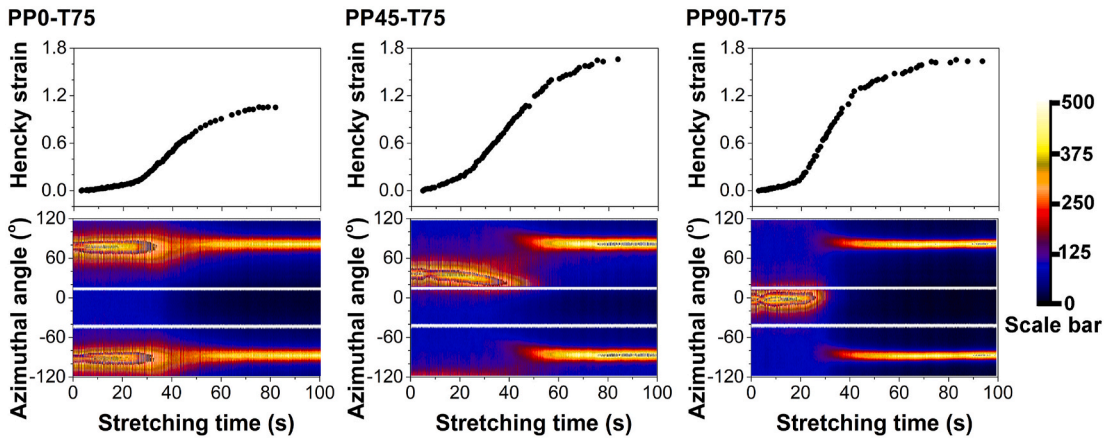

Fig. 2. The intensity distribution of (040) crystal plane in the azimuthal direction upon stretching.

that DA is 45°, and the stretching temperature is 75 °C.

The in-situ WAXS experiments were made up of two parts: (1) the first part was performed at the MiNaXS Beamline at Deutsches Elektronen Synchrotron (Hamburg, Germany). The beam size was 23 μm × 13 μm. The X-ray wavelength was 0.92475 Å. The exposure time and waiting time were 0.1 s and 0.15 s, and a Pilatus 300K detector (487 × 619 pixels) were used to record the pattern. The distance between the sample and the detector was 210 mm. The stretching was performed on a custom-made miniature tensile machine [36] with a stretching speed of 0.02 mm/s. PP0-T75, PP45-T75, PP90-T75 were tested in this part, and stretching was continuously performed during WAXS pattern recording. Additionally, a stress relaxation test was performed on PP0-T75 at 75 °C after the specimen was stretched, and the structural evolution during relaxation was recorded; (2) the second part was performed on D8 ADVANCE (Bruker, Germany) diffraction instrument with Vantec 500 area detector (2048 × 2048 pixels). The radius of the beam size was 500 μm. The wavelength was 1.54 Å, the exposure time was 30 s and the waiting time was 5 s. The stretching was performed on TST350 tensile stage (Linkam, U.K.) with a stretching speed of 0.02 mm/s. In this part, PP45-T0, PP45-T15, PP45-T45, PP45-T75, PP45-T90, PP45-T105, PP45-T120, PP45-T135, and PP45-T150 were tested, and stretching was stopped during WAXS pattern recording. The WAXS patterns were background corrected and processed by self-written Python scripts.

The macroscopic Hencky strain (ε_H) at the position where X-ray past

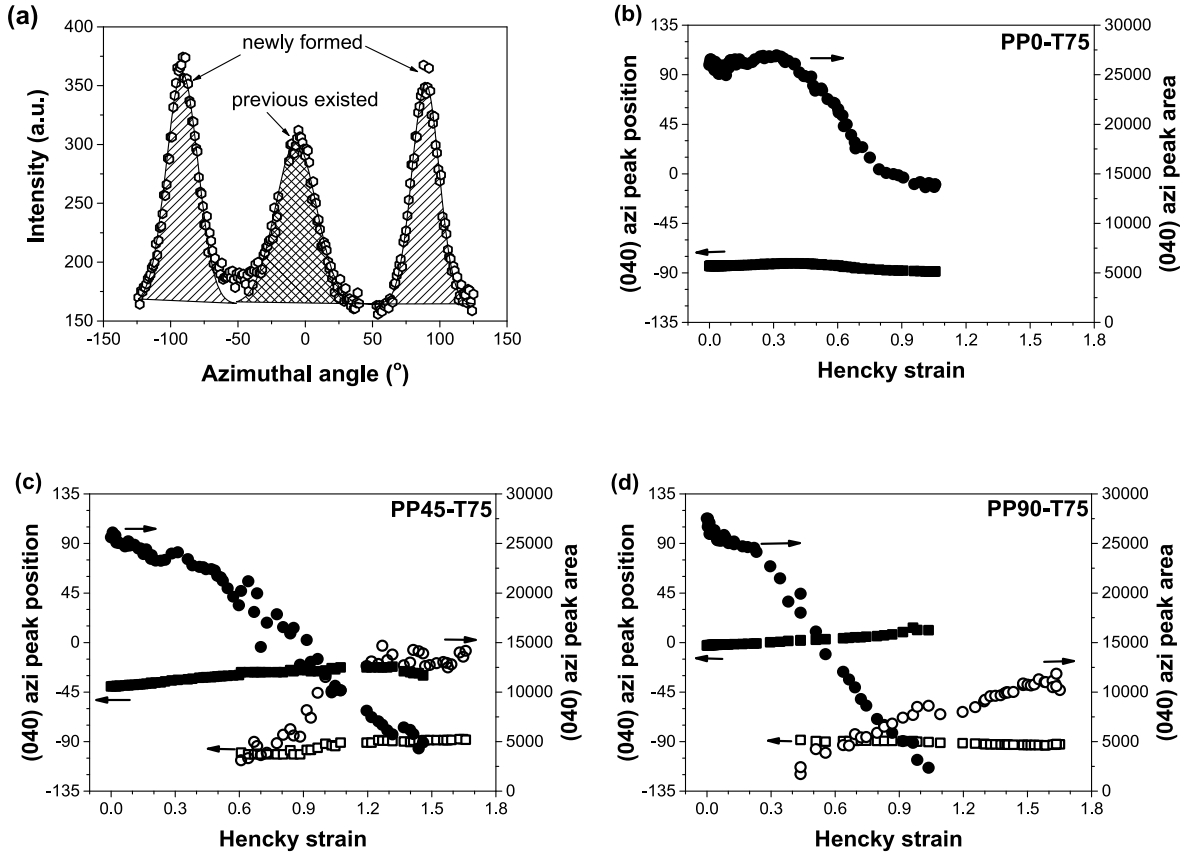

Fig. 3. Schematic illustration of the peak fitting procedure of the azimuthal intensity distribution curve of (040) crystal plane (a); The evolution of the peak position and peak area of (040) crystal plane in PP0-T75 (b), PP45-T75 (c), and PP90-T75 (d). The peak position is represented by square, and the peak area is represented by circle. In addition, the position and area of the previous existed peak are solid symbol, the position and area of the newly formed peak are open symbol.

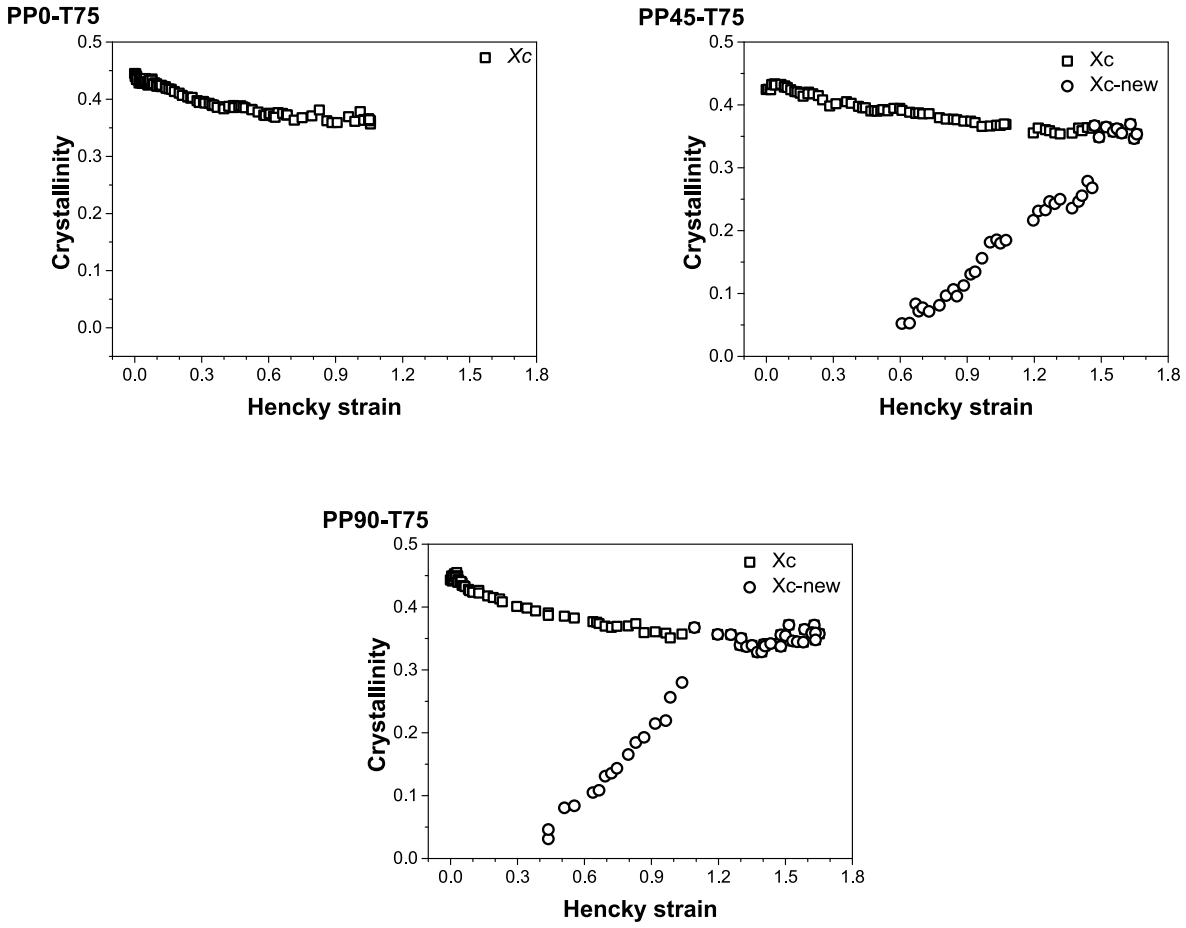

Fig. 4. The evolution of the total crystallinity X_c (square) and the crystallinity of newly formed crystal X_{c-new} (circle) with Hencky strain.

was assessed by

$$\varepsilon_H = 2ln\frac{b_0}{b} \tag{1}$$

where b_0 and b were the initial width and the width during stretching. The background for using the Hencky strain instead of the engineering strain is that the Hencky strain is additive and taking the increasing length of the element during stretching into consideration [37].

3. Results and discussion

3.1. Influence of DA on the crystallization behavior

The stress-strain curves of PP0-T75, PP45-T75, and PP90-T75 are presented in Fig. 1, as well as some representative WAXS patterns during stretching. The number located at the left corner marks the ε_H when the pattern was taken.

The stress-strain curve is divided into a linear deformation before yielding, the strain softening, the plateau region, and lastly the strain hardening. Taking PP0-T75 as an example, stress increased linearly as ε_H was smaller than 0.05. The linear increment was associated with the affine deformation of the microstructure [38]. After the strain softening, a plateau appears where stress grew only slightly in a quite large strain range (0.05–1.0). In the last part ($\varepsilon_H > 1.0$), the strain-hardening appeared where a stress upturn showed up in a very sharp way. The strain hardening was caused by the extension saturation of the chains network cross-linked physically or by micro-crystallite [16,18,39]. As DA was changed from 0° to 90°, the evolution trend of the stress as a function of ε_H was generally the same, but the onset strain of the strain hardening was postponed obviously, indicating a different microstructure development in the specimen before strain hardening.

On the WAXS pattern, a few arcs can be recognized from inner to outer, which are the reflections from (110), (040), (130), (111), and (−131) crystal planes of α-iPP. On the unstretched WAXS pattern, a weak (300) reflection between (110) and (040) reflections can be found, indicating the existence of a trace amount of β-iPP. Since that the content of β-iPP is quite low (~0.03), so its deformation is ignored in this work. The deformation behavior of iPP with high content of β-iPP can be found in other studies [40–42] as well as our previous report [43].

According to the intensity distribution of the (110) crystal plane, the peculiar "cross-hatched" structure of α-iPP can be recognized [44]. In PP0-T75, before stretching the *c*-axis of the "mother" part of the "cross-hatched" structure was parallel with the stretching direction, and the *c*-axis of the "daughter" part was inclined 80° to the stretching direction. Upon stretching, the scattering intensity of the "daughter" part weakened gradually, and the intensity of the "mother" part was enhanced. In addition, the orientation degree of the "mother" part was strengthened. Whereas, in PP45-T75 and PP90-T75 the scattering intensity of "mother" part was weakened obviously (Fig. S2). Moreover, in PP45-T75 and PP90-T75 a new arc appeared on (040) reflection (marked by green arrows in Fig. 1) as ε_H exceeded 0.8, indicating that in addition to the previously existed crystal a new group of crystal was formed upon drawing. The newly formed arc was located close to the meridian suggesting that the *b*-axis of the newly formed crystal was perpendicular to the stretching direction.

The formation of the new crystal is of great possibility caused by the stretching of polymer chains in the amorphous phase rather than the melting of the initially existed crystal, as evidenced by the coexistence of previous crystal and newly formed crystal in a specific drawing regime. Whereas, more evaluation should be performed before a conclusion can

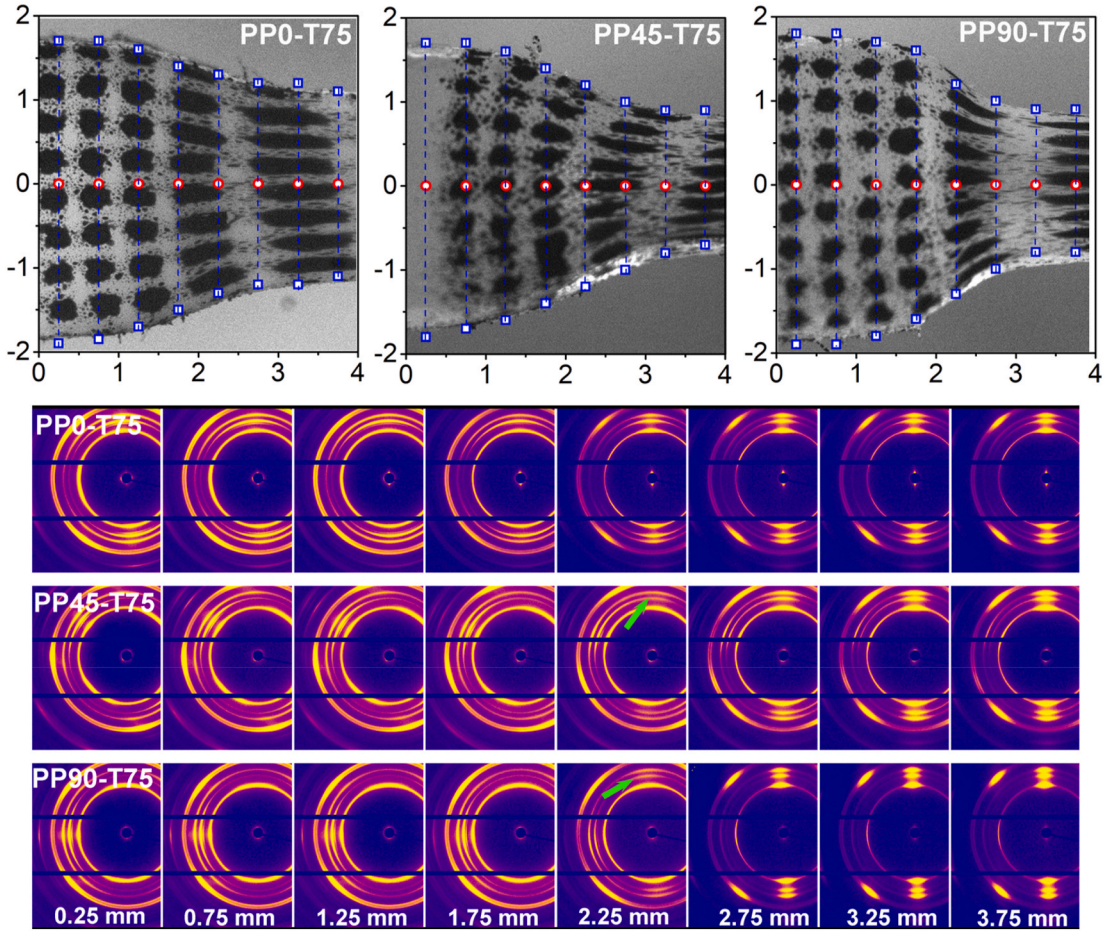

Fig. 5. The optical image of the specimen stretched at 75 °C, and representative 2D-WAXS patterns taken from the red dots. (For interpretation of the references to colour in this figure legend, the reader is referred to the Web version of this article.)

be made. Fig. 2 presents a vivid presentation of (040) intensity distribution in the azimuthal direction during stretching. One can see that as DA was 45° and 90°, the formation of the new group of crystals was clearly presented, providing us an opportunity to quantitatively evaluate the crystallization process.

A representative azimuthal intensity distribution curve of (040) crystal plane is plotted in Fig. 3a. Since that an azimuthal angle range of −125°~125° is chosen, so only three peaks can be found with the middle one originated from the previous existed crystal and the other two ascribed to the newly formed crystal. The peak position and peak area were obtained by a peak fitting procedure using the Gaussian function. The change of the peak position and peak area were summarized in Fig. 3b~(d). The peak position is represented by square, and the peak area is represented by circle. In addition, the position and area of the previous existed peak are solid symbol, the position and area of the newly formed peak are open symbol.

One can see that in PP0-T75, as the ε_H was smaller than 0.45 the peak position shifted very slightly, afterward the peak position decreased gradually from −92° to −90° and finally stayed unchanged as the ε_H exceeds 0.8. Meanwhile, an obvious decrease of the peak area occurred at the ε_H of 0.33, and the decrease of the peak area slowed down when the ε_H was larger than 0.8. The decrease of the peak area can be caused by both crystal fragmentation and the thinning of the specimen's thickness. In PP45-T75, the peak position increased continuously with the ε_H, as a result of the lamellar slip and chain slip which has been evidenced in our previous study [33]. Additionally, the peak area was reduced drastically as the ε_H is larger than 0.5. When the ε_H was larger than 0.6, the peak originated from the newly formed crystal showed up. The peak position of the newly formed crystal was around −100° at the very beginning and changed gradually to −90°. The peak area exhibited a linear increasing trend with the ε_H and reached a plateau in the late stage of stretching. In PP90-T75, the peak position was changed slightly during the whole stretching, and the drastic decrease of the peak area presented at a smaller ε_H compared with that in PP45-T75. Similarly, the scattering of the newly formed crystal appeared at a smaller ε_H. The peak position of the new scattering was located at −90° in the whole stretching.

For polymer materials, the peak area is generally regarded as the "total peak intensity" since the area represents the true sum of all the diffracted X-rays that have been scattered by all crystals. Therefore, the peak area was adopted for the calculation of the crystallinity of newly formed crystal (X_{c-new}). The detailed calculation procedure can be found in the Supporting Information, and the results are summarized in Fig. 4. One can see that X_c of PP0-T75, PP45-T75, and PP90-T75 was decreased gradually in the whole stretching process, as a result of chain slip, lamellae fragmentation, and melting-recrystallization. Whereas, as DA was 45° or 90°, the crystallization process of the newly formed crystal could be clearly "visualized". To be more specific, X_{c-new} presented a linear dependence on Hencky strain. In PP45-T75, X_{c-new} arose at an ε_H of 0.6 and overlaps with X_c as ε_H was larger than 1.5. In PP90-T75, X_{c-new} showed up at an ε_H of 0.44 and reached the plateau at an ε_H of 1.1.

3.2. The spatial distribution of the newly formed crystal in the neck

To check the spatial distribution of the newly formed crystal in the neck, a few vertical scans were performed by the micro-beam

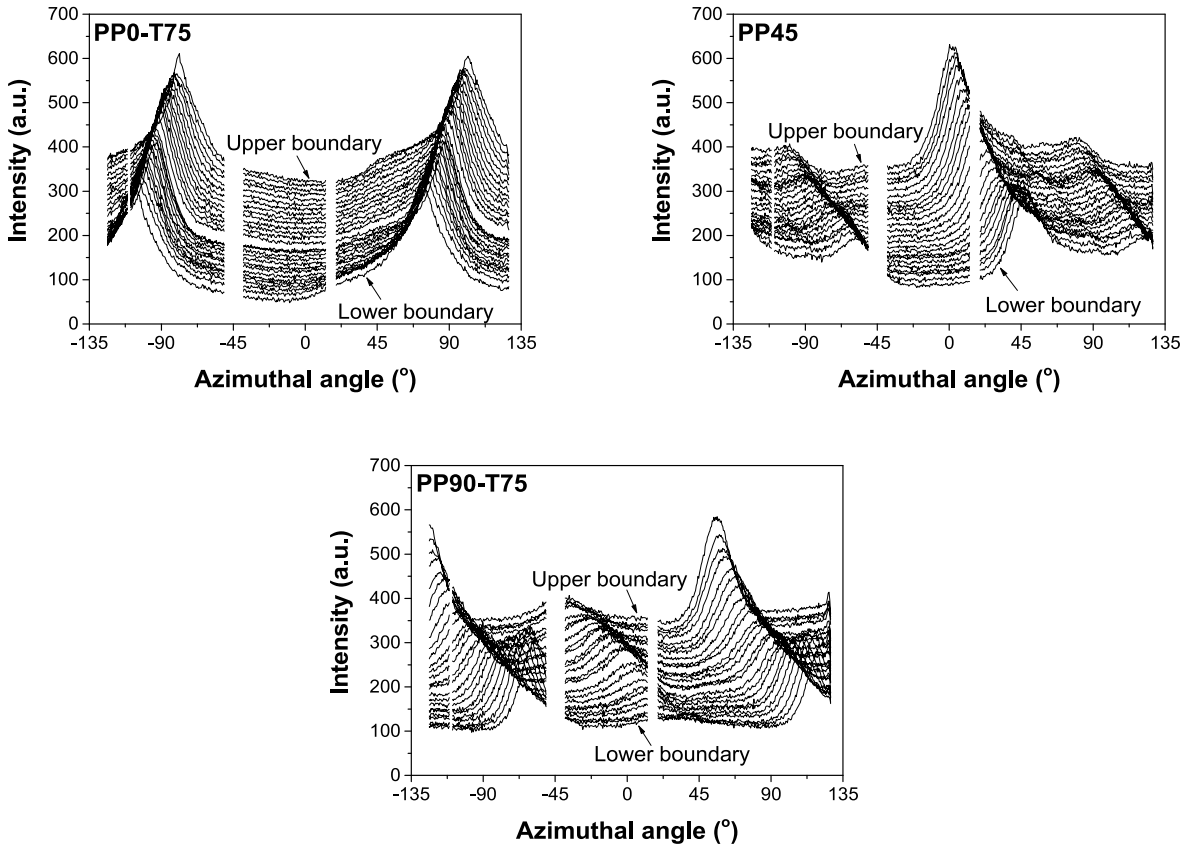

Fig. 6. The intensity distribution of the (040) crystal plane of the whole vertical scan at the horizontal position of 2.25 mm "Upper boundary" and "Lower boundary" mean that the curve is taken from upper and lower boundary of the specimen in the vertical scan.

synchrotron WAXS. The step in the vertical scan was 0.1 mm and the step between the vertical scan was 0.5 mm. Due to the absorption of the X-ray by the specimen, the boundary of the neck can be easily determined by the intensity ratio of the X-ray before and after specimen (Fig. S3 in the **Supporting Information**). Fig. 5 shows some representative 2D-WAXS patterns taken from the red dots. As one can see, in PP0-T75 the intensity distribution of (040) reflection was narrowed obviously at a horizontal position of 2.25 mm The narrowed arc is a combination of the previously existed signal and the newly formed signal. Meanwhile, on the meridian a new signal (indicated by the green arrow) can be found in PP45-T75 and PP90-T75, in addition to previously existed signal located at 49° and 0°, respectively. As the horizontal position moves to 2.75 mm, the new signal becomes the dominating one. Note that the size of the beam is 23 μm × 13 μm, the results here proves that the crystallization process occurs in a very narrow spatial region.

Furthermore, the intensity distribution of (040) reflection in the whole vertical scan at the horizontal position of 2.25 mm is plotted in Fig. 6. "Upper boundary" and "Lower boundary" donate that the curve is taken from the upper and lower boundary of the specimen in the vertical scan. In PP0-T75, the scattering peak of the newly formed crystal is overlapped with that of the previous crystal. In PP45-T75 and PP90-T75, the peak caused by the newly formed crystal can be easily recognized. In PP90-T75, the peak area of the newly formed crystal is smaller in the boundary region, suggesting that the crystallization process is very weak therein, which is probably related to the strain variation in the vertical scan. From upper to lower boundary, the peak position is shifted

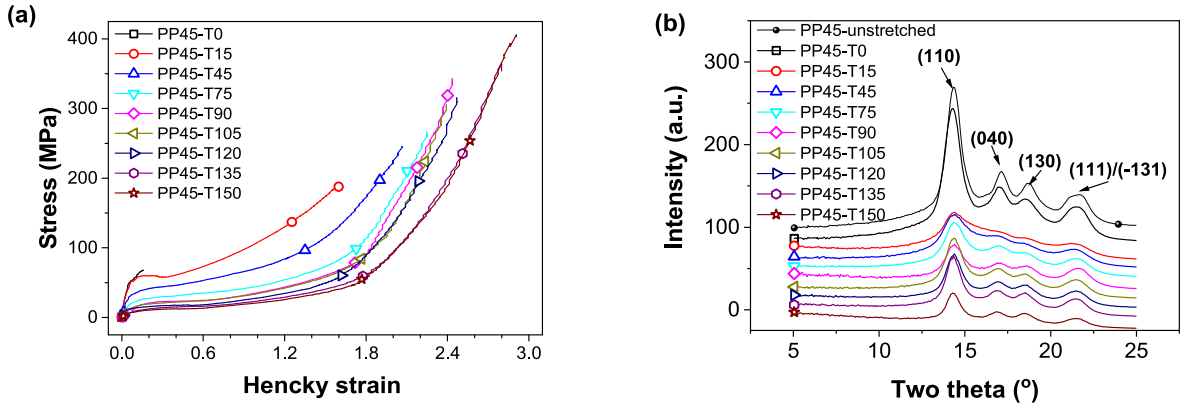

Fig. 7. (a) The stress-strain curves of PP45 stretched at different temperatures; (b). The 1D-WAXS curves at the final stage of stretching. For comparison, the curve of the unstretched sample is also provided.

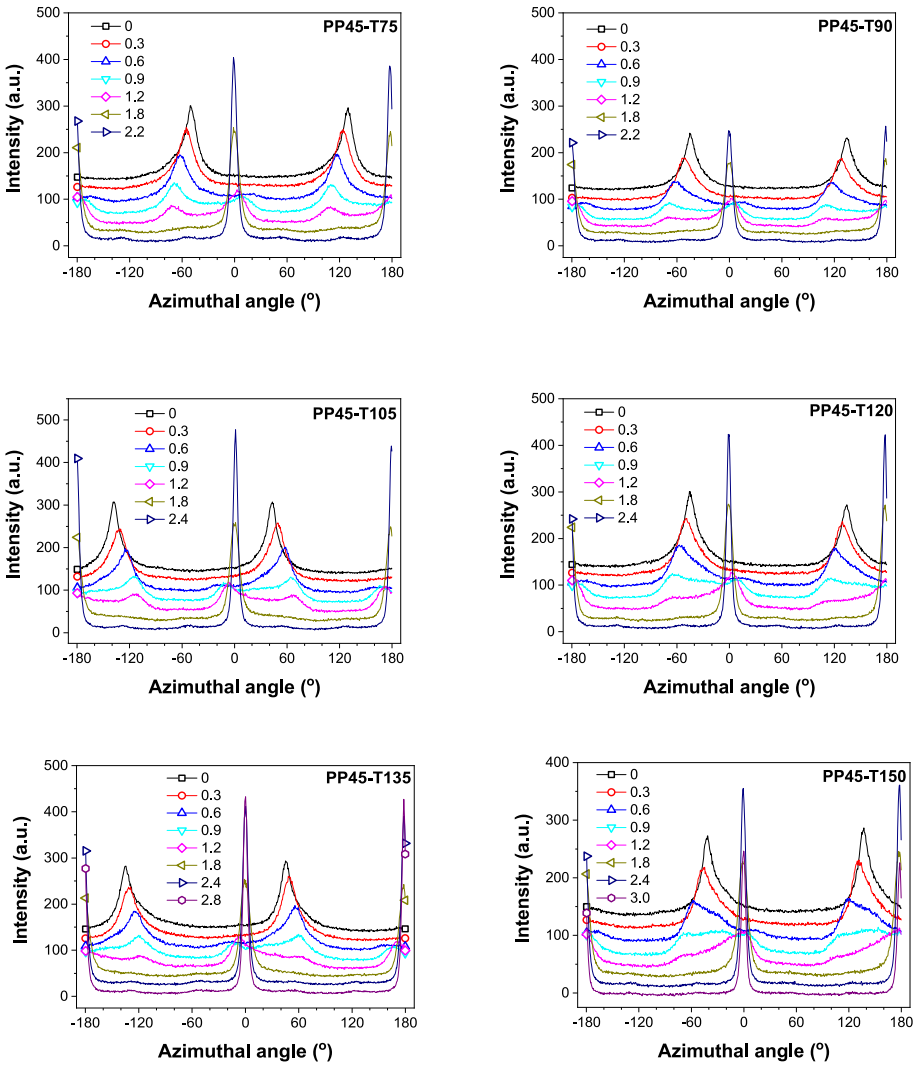

Fig. 8. The azimuthal intensity distribution of (040) reflection during stretching. The stretching temperature can be found from the marks at the corner of the figure.

gradually, indicating that the orientation of the curve is determined by the principle stress it suffered. In addition, the peak position is shifted toward a single direction, since that the direction of the principle stress in the neck owns a axial symmetry with respect to the stretching direction.

3.3. *Influence of stretching temperature on the crystallization behavior*

As mentioned in the introduction part, the stretching temperature is a key factor influencing the crystallization behavior during stretching. To figure out the role of stretching temperature on the evolution of X_{c-new}, DA was fixed at 45° and a temperature range of 0–150 °C was used. The stress-strain curves of PP45 stretched at different temperatures are shown in Fig. 7a. All samples presented a cold drawing except for PP45-T0, which exhibited a brittle fracture behavior. In general, higher stretching temperature led to smaller yield stress and longer elongation at break. The 1D-WAXS curves at the final stage of stretching are given in Fig. 7b. For comparison, the 1D-WAXS curve of the unstretched sample is also provided. The 1D-WAXS curve of PP45-T0 is nearly the same as the unstretched one, suggesting that no crystallization happened when the sample was fragmented in a brittle way. In PP45-T15, the (040) peak was blurred by a broad peak originated from the formation of mesophase. In PP45-45, both mesophase and α-iPP existed. The mesophase disappears when the stretching temperature was higher than 75 °C. The formation of mesophase at low temperature coincides very well with other reports [29,45–48]. Since that the interest in this work is focused on the crystallization behavior during stretching, so only those samples stretched at a temperature higher than 75 °C will be further analyzed.

Representative curves of (040) crystal plane are shown in Fig. 8. Generally, the evolution of the azimuthal intensity distribution showed a similar trend as the stretching temperature was elevated. Taking PP45-T150 as an example, before stretching, two characteristic peaks located at −45° and 135° could be found on the curve. Upon stretching, the peaks shifted to a smaller value as a result of lamellae slip and chain slip. As the Hencky strain exceeded 0.6, a new peak at −10° showed up, indicating the occurrence of crystallization. The intensity of the newly formed peak became stronger with further stretching. As the Hencky strain was larger than 1.6, the peak of the previous crystal disappeared totally and the new scattering became narrower and higher. The position of the new scattering stayed at *ca.* 0°, suggesting that the ***b***-axis of the newly formed crystal was perpendicularly oriented to the stretching direction. The orientation factor of the ***b***-axis calculated by Hermann's method is *ca* −0.34 regardless of the stretching temperature.

The evolution of X_c and X_{c-new} of PP45 stretched at temperatures from 75 °C to 150 °C with an interval of 15 °C are given in Fig. 9. It should be pointed out that before stretching, a decrease of X_c can be seen as a result of temperature-induced melting. Compared with that of the specimen stretched at 75 °C, the crystallinity of the specimen stretched at 150 °C was decreased by 15%. Upon stretching, the change of X_c

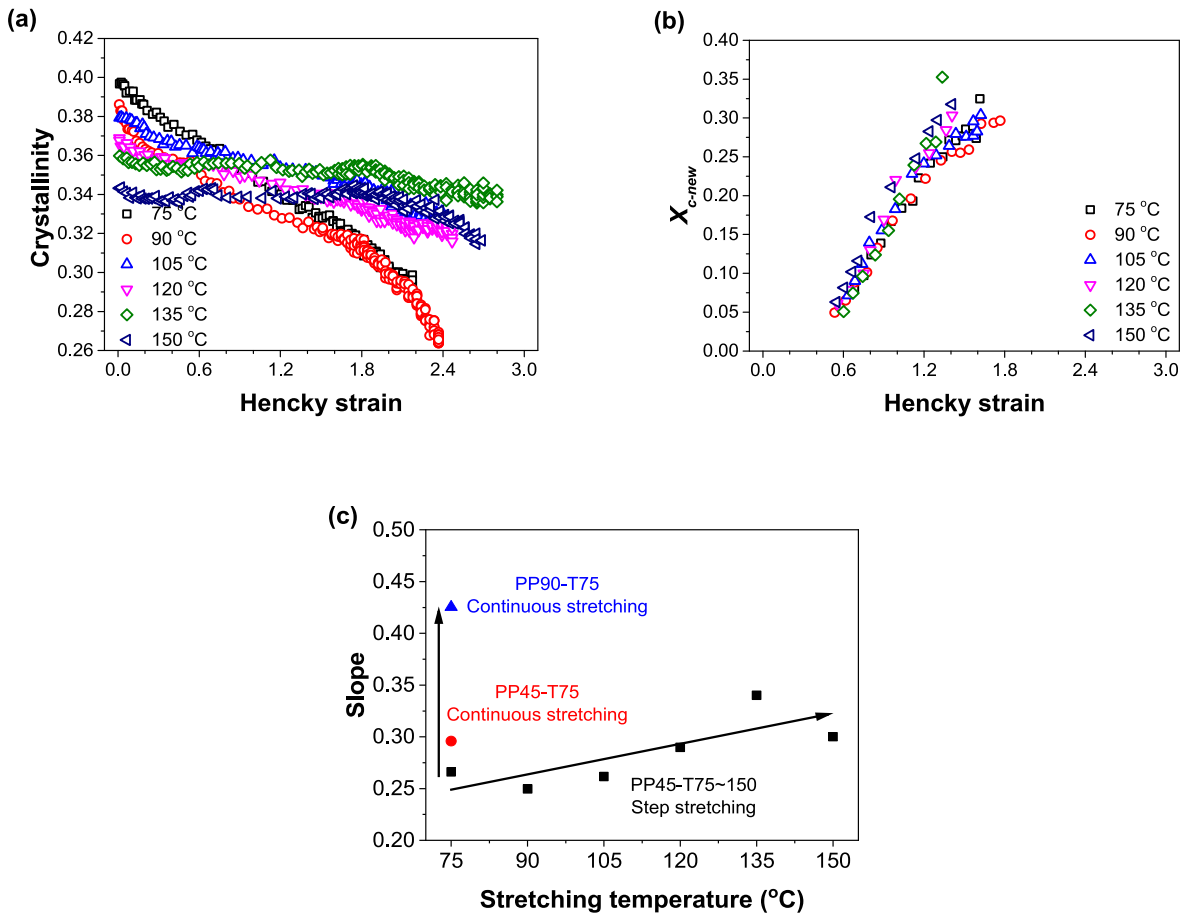

Fig. 9. The evolution of (a) X_c and (b) X_{c-new} with increasing Hencky strain of PP45 stretched at different temperatures; (c) The slope of the plot of X_{c-new} as a function of the Hencky strain, the black squares are PP45 stretched in a step way at 75 °C, 90 °C, 105 °C, 120 °C, 135 °C, and 150 °C, the red circle is PP45-T75 stretched continuously, and the up triangle is PP90-T75 stretched continuously. (For interpretation of the references to colour in this figure legend, the reader is referred to the Web version of this article.)

differed greatly as the stretching temperature was elevated. For the specimen stretched at 75 °C, X_c was decreased continuously with stretching. As the temperature was elevated to 120 °C, only a mild decrease of X_c can be found. With a stretching temperature of 150 °C, X_c was kept nearly unchanged until the Hencky strain of 2.0. Surprisingly, in Fig. 9b it can be found that X_{c-new} exhibited a similar increasing trend for the specimen stretched at a temperature range of 75–150 °C, suggesting that the different decreasing trend of X_c was mainly caused by the deformation and melting of the previous structure. The slope of the plot of X_{c-new} as a function of Hencky strain is summarized in Fig. 9c. Compared with the stretching temperature, the slope of the plot is more sensitive to DA. As DA was increased from 45° to 90°, the slope was enlarged 43% from 0.30 to 0.43. However, as the stretching temperature was increased from 75 °C to 150 °C, the slope was changed only slightly from 0.27 to 0.30. In addition, compared with continuously stretching, the slope of the plot was slightly smaller when the specimen was stretched in a step way.

3.4. The mechanism responsible for the crystallization process during solid-state stretching

As presented by the results in previous parts, the crystallization behavior of partially oriented iPP during solid-state stretching can be easily monitored if the stretching direction biases the initial orientation direction. More importantly, X_{c-new} shows a linear dependence on the Hencky strain, and the slope of the plot is more sensitive to DA instead of the stretching temperature. The crystallization occurs in the plateau region which is later than the yielding but earlier than the strain hardening (Figs. 1 and 7a). In this region, the stress is enlarged only slightly in a quite wide strain range, indicating that the crystallization is dominated by macroscopic Hencky strain.

As a matter of fact, strain-induced crystallization was frequently encountered in polyester (poly(ethylene terephthalate) [49], poly (ethylene furanoate) [50], poly(ethylene 2,5-furandicarboxylate)) [51,52] when stretching above its α_c relaxation temperature [50,53], or rubber (natural rubber [54], poly(dimethylsiloxane) [55], polychloroprene [56,57]) above its glass transition temperature. The strain-induced crystallization is a very fast process [58,59]. Half of the crystallization process completes within less than 5 ms as long as the strain is large enough [59]. The size of the local ordering is characterized by two length scales (~4 Å and ~2 Å) in poly(ethylene furanoate), associated with the lateral inter-chain distance and staggering along the polymer chain direction, respectively [50]. The prerequisite for strain-induced crystallization is the local ordering of chains with preferred orientation caused by stretching. The thermodynamic driving force for strain induced crystallization is proposed by Flory [60]: firstly, lowering of the entropy cost by incorporating the pre-stretched polymer chain segments into crystallites; secondly, releasing the entropy into the amorphous phase adjacent to the crystal, which promotes the growth of the crystallites. The entropy release by orientation relaxation has already been verified experimentally in natural rubber [61] and polychloroprene rubber [57].

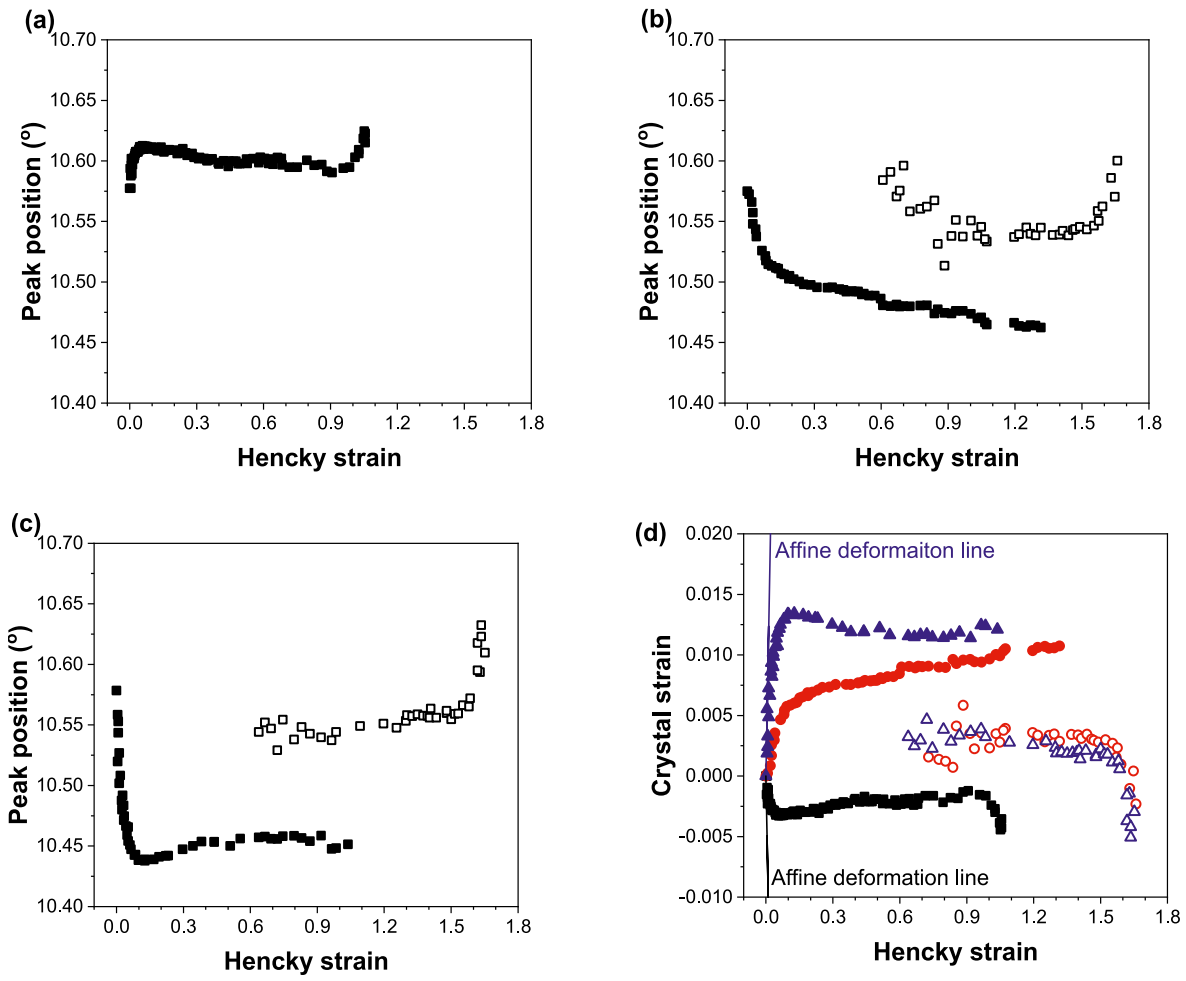

Fig. 10. The peak position of (040) crystal plane in the radial direction of (a) PP0-T75, (b) PP45-T75, and (c) PP90-T75; (d) The crystal strain of PP0-T75 (square), PP45-T75 (circle), and PP90-T75 (up triangle). In Fig. 10d, the solid symbol represents the value of previously existed crystal, and the empty symbol represents the value of newly formed crystal.

3.4.1. *The local strain state of the crystal during stretching*

Different from polyester or rubber which are amorphous before strain-induced crystallization, abundant crystalline structures exist in iPP before crystallization. Therefore, to figure out the microscopic physical process of the strain-induced crystallization in iPP, the deformation of its initial structure should be considered. As has been widely reported, the deformation of the semicrystalline polymer during cold-drawing is realized by chain slip, lamellae slip, fragmentation of lamellae into blocks and lamellae block rotation at small deformation [13–22].

In our previous work, the deformation of PP0-T75, PP45-T75, and PP90-T75 was systematically investigated by in-situ synchrotron SAXS and WAXS. It was found that in the elastic deformation region of PP0-T75 and PP90-T75, no slip process happens, and the amorphous phase between lamellae suffered a stretching or compression stress respectively. Whereas in the elastic deformation region of PP45-T75, both lamellae slip and chain slip exist. In the strain softening region after yielding, lamellae are fragmented into blocks for PP0-T75, PP45-T75, and PP90-T75.

Since that the crystallization process happened in the region later than the yielding and earlier than the strain hardening, so the local strain state in this region should be further analyzed. The local strain on the crystal ($\varepsilon_{(hkl)}$) was calculated as follows

$$\varepsilon_{(hkl)} = \frac{d_{(hkl)} - d^0_{(hkl)}}{d^0_{(hkl)}} \tag{2}$$

$$d_{(hkl)} = \lambda / 2sin\theta \tag{3}$$

with $d_{(hkl)}$ is the *d*-spacing of the (hkl) crystal plane during stretching, $d^0_{(hkl)}$ is the *d*-spacing before deformation, λ is the wavelength.

The peak position in the radius direction of the (040) crystal plane is provided in Fig. 10a–c. One can see that in PP0-T75, the peak position showed a sudden increase in the elastic deformation region, afterward, it was changed only slightly. At the end of stretching, the peak position moved obviously to a larger value due to strain hardening. In PP45-T75 and PP90-T75, the sudden decrease of peak position can be found in the elastic deformation. Furthermore, the peak position of the newly formed crystal was kept at *ca.* 10.55 once it was formed. The crystal strain on the previously existed crystal (solid symbol) and newly formed crystal (empty symbol) is presented in Fig. 10d. It can be seen that the affine deformation ends quickly as the deformation exceeds the elastic region. In the non-affine deformation, the stretching of the specimen was realized by the extension of the polymer chains network between fragmented lamellae blocks. In addition, due to the co-existence of lamellae slip and chain slip, the local crystal strain in PP45-T75 was smaller than that in PP90-T75. Interestingly, the local crystal strain on the newly formed crystal was nearly the same in PP45-T75 and PP90-T75, which was much smaller than that on the previously existed crystal. Adopting the two-phase model to represent the structural element of iPP, the results here suggest that compared with the molecular chains adjacent to the previously existed crystal, those adjacent to the newly formed crystal

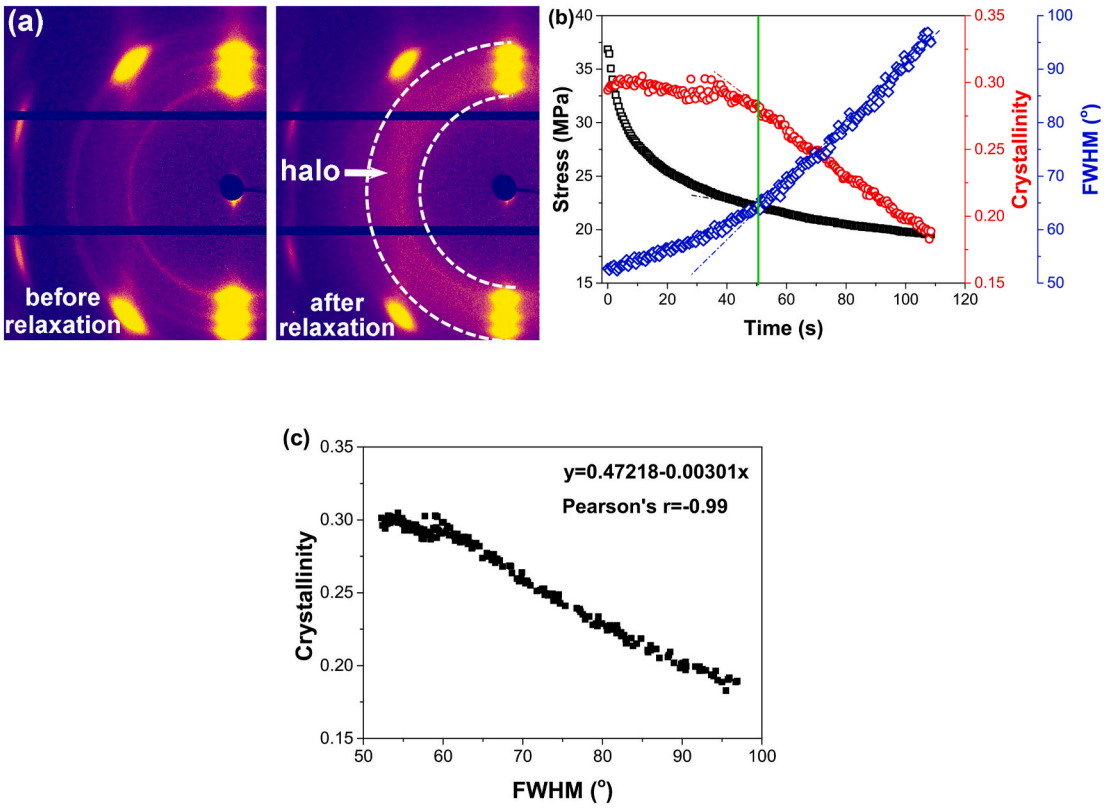

Fig. 11. (a) Selective 2D-WAXS patterns before and after relaxation. The temperature of the stress relaxation was 75 °C; (b) the macroscopic stress, the crystallinity, and the full width at half maximum (FWHM) of the specimen during relaxation; (c) the plot of crystallinity as a function of FWHM.

own a much smaller extension.

3.4.2. *The decreasing of the crystallinity during stress relaxation*

The results in Fig. 10 demonstrate that during solid-state stretching, the affine deformation ends quickly. As the crystallization took place, the local crystal strain was far smaller than the macroscopic strain, implying that the chain network in the amorphous phase should be greatly stretched. To get further insight into the relationship between the chain network orientation and the crystallization process, a stress relaxation experiment was performed at 75 °C. Before relaxation, the specimen was stretched to a Hencky strain of 1.2. Selective 2D-WAXS patterns before and after relaxation is provided in Fig. 11a. The 1D-WAXS curve circularly integrated from the 2D-WAXS pattern proves substantially that upon relaxation the intensity of the crystalline peaks was decreased while that of the amorphous part was enhanced (Fig. S5a). To track the evolution of the amorphous phase during relaxation, the intensity distribution in the white annular region is provided in Fig. S5b. Then the intensity plot was deconvolved into amorphous part and crystalline part by a peak fitting procedure using Gaussian function. The crystallinity obtained from Fig. S5a and the full width at half maximum (FWHM) of the amorphous part obtained from Fig. S5b are summarized in Fig. 11b. It can be found that the stress decayed exponentially with time and it dropped very fast in the first 7 s, whereas the crystallinity and the FWHM were changed only slightly. As the relaxation time was larger than 51 s, the crystallinity was decreased obviously and the FWHM was increased drastically. The plot of the crystallinity as a function of FWHM (Fig. 11c) shows that the linear correlation coefficient (Pearson's r) between them is as high as −0.99, proving that the crystallization of iPP in the solid-state is determined principally by the chain network orientation in the amorphous phase.

Since that the crystallization process is dominated by the strain-induced orientation of the chain network connected by physical cross-linking points or crystallites, the slope of the plot will be influenced by the state of the network. As revealed by Candu et al. [62], The slope of the plot was a function of the density of the elastically active chain between cross-linking points. As the density of the elastically active chains was continuously enlarged, the slope of the plot in rubber would first increase and then decreases [63]. The existence of an optimum value of the density of active chains between cross-linking points was also verified by Tosaka et al. [64] In addition, the heterogeneities of the polymer chain network will also influence the crystallization process, since that the crystallization can be triggered with only small portions of the chains to orient while the other chains stay randomly coiled [65]. In our case, before crystallization, the deformation of lamellae was dominated by lamellae and chain slip in PP45-T75, and by chain slip in PP90-T75, respectively. It can be inferred that the different deformation processes gave rise to a different active chain density. Therefore, the slope of the plot is different in PP45-T75 and PP90-T75.

4. Conclusion

In this study, partially oriented isotactic polypropylene (iPP) is used as a template material to study the crystallization behavior during solid-state stretching. The structural evolution during stretching is in-situ monitored by wide-angle X-ray scattering (WAXS). Using the intensity distribution of (040) reflection as a designator, the relationship between the crystallinity of the newly formed crystal and the macroscopic Hencky strain is discussed. Results showed that the crystallinity of the newly formed crystal shows a linear dependence on the macroscopic Hencky strain, and the slope of the plot is more sensitive to the stretching angle rather than the stretching temperature. The crystallization happens in the regime later than the yielding but earlier than the strain hardening. In this regime the stress is increased only slightly in a quite large strain range. In addition, the crystal strain in this regime is much smaller than the macroscopic Hencky strain, suggesting that the chain network in the amorphous phase is greatly stretched when

crystallization takes place. The stress relaxation test further shows that the crystallinity is linear correlated to the amorphous phase orientation, and the Pearson correlation coefficient is as high as −0.99, suggesting that the orientation of the chain network is the prequiste for the crystallization process during solid-state stretching.

Author contributions

The manuscript was written through contributions of all authors. All authors have given approval to the final version of the manuscript.

Declaration of competing interest

The authors declare that they have no known competing financial interests or personal relationships that could have appeared to influence the work reported in this paper.

Acknowledgement

The authors are grateful to DESY for beamtime within the project II-20150042. Baobao Chang gratefully acknowledges the financial support for this work by the National Natural Science Foundation of China (grant no. 52003249), the China Postdoctoral Science Foundation (grant no. 2019M652571), the Natural Science Foundation of Henan (grant no. 202300410426), the Open Funding Project of National Key Laboratory of Human Factors Engineering (grant no. SYFD061910K).

Appendix A. Supplementary data

Supplementary data to this article can be found online at https://doi.org/10.1016/j.polymertesting.2021.107404.

References

[1] H. Staudinger, Über polymerisation, Ber. Dtsch. Chem. Ges. 53 (1920) 1073–1085.
[2] C.Y. Li, The rise of semicrystalline polymers and why are they still interesting, Polymer 211 (2020) 123150.
[3] S.J. Rowan, Happy 100th anniversary to polymer science and engineering, ACS Macro Lett. 9 (2020), 122-122.
[4] H. Wang, J.K. Keum, A. Hiltner, E. Baer, B. Freeman, A. Rozanski, A. Galeski, Confined crystallization of polyethylene oxide in nanolayer assemblies, Science 323 (2009) 757–760.
[5] M. Vatankhah-Varnosfaderani, W.F.M. Daniel, M.H. Everhart, A.A. Pandya, H. Liang, K. Matyjaszewski, A.V. Dobrynin, S.S. Sheiko, Mimicking biological stress–strain behaviour with synthetic elastomers, Nature 549 (2017) 497–501.
[6] Y. Zhu, C. Romain, C.K. Williams, Sustainable polymers from renewable resources, Nature 540 (2016) 354–362.
[7] C. De Rosa, C. Park, E.L. Thomas, B. Lotz, Microdomain patterns from directional eutectic solidification and epitaxy, Nature 405 (2000) 433–437.
[8] P.D. Coates, I.M. Ward, Drawing of polymers through a conical die, Polymer 20 (1979) 1553–1560.
[9] G. Capaccio, I.M. Ward, Preparation of ultra-high modulus linear polyethylenes; effect of molecular weight and molecular weight distribution on drawing behaviour and mechanical properties, Polymer 15 (1974) 233–238.
[10] L.E. Govaert, T. Peijs, Tensile strength and work of fracture of oriented polyethylene fibre, Polymer 36 (1995) 4425–4431.
[11] Y. Lin, R. Patel, J. Cao, W. Tu, H. Zhang, E. Bilotti, C.W.M. Bastiaansen, T. Peijs, Glass-like transparent high strength polyethylene films by tuning drawing temperature, Polymer 171 (2019) 180–191.
[12] L. Shen, K. Nickmans, J. Severn, C.W.M. Bastiaansen, Improving the transparency of ultra-drawn melt-crystallized polyethylenes: toward high-modulus/high-strength window application, ACS Appl. Mater. Interfaces 8 (2016) 17549–17554.
[13] P.B. Bowden, R.J. Young, Deformation mechanisms in crystalline polymers, J. Mater. Sci. 9 (1974) 2034–2051.
[14] R.J. Young, P.B. Bowden, J.M. Ritchie, J.G. Rider, Deformation mechanisms in oriented high-density polyethylene, J. Mater. Sci. 8 (1973) 23–36.
[15] A. Peterlin, Drawing and extrusion of semi-crystalline polymers, Colloid Polym. Sci. 265 (1987) 357–382.
[16] A. Peterlin, Molecular model of drawing polyethylene and polypropylene, J. Mater. Sci. 6 (1971) 490–508.
[17] L. Lin, A.S. Argon, Structure and plastic deformation of polyethylene, J. Mater. Sci. 29 (1994) 294–323.
[18] R. Hiss, S. Hobeika, C. Lynn, G. Strobl, Network stretching, slip processes, and fragmentation of crystallites during uniaxial drawing of polyethylene and related copolymers, A comparative study, Macromolecules 32 (1999) 4390–4403.
[19] A. Pawlak, A. Galeski, Plastic deformation of crystalline polymers: the role of cavitation and crystal plasticity, Macromolecules 38 (2005) 9688–9697.
[20] K. Nitta, T. Kawada, M. Yamahiro, H. Mori, M. Terano, Polypropylene-block-poly (ethylene-co-propylene) addition to polypropylene/poly(ethylene-co-propylene) blends: morphology and mechanical properties, Polymer 41 (2000) 6765–6771.
[21] Y. Men, Critical strains determine the tensile deformation mechanism in semicrystalline polymers, Macromolecules 53 (2020) 9155–9157.
[22] Y.-G. Zhou, L.-S. Turng, C.-Y. Shen, Morphological evolution and orientation development of stretched iPP films: influence of draw ratio, J. Polym. Sci. B Polym. Phys. 48 (2010) 1223–1234.
[23] Y. Wang, Z. Jiang, L. Fu, Y. Lu, Y. Men, Stretching temperature dependency of lamellar thickness in stress-induced localized melting and recrystallized polybutene-1, Macromolecules 46 (2013) 7874–7879.
[24] Y. Lu, Y. Wang, L. Fu, Z. Jiang, Y. Men, Crystallization, recrystallization, and melting lines in syndiotactic polypropylene crystallized from quiescent melt and semicrystalline state due to stress-induced localized melting and recrystallization, J. Phys. Chem. B 118 (2014) 13019–13023.
[25] Y. Lu, Y. Wang, R. Chen, Y. Men, Crystallization and melting of isotactic polypropylene crystallized from quiescent melt and stress-induced localized melt, J. Polym. Sci. B Polym. Phys. 55 (2017) 957–963.
[26] L. Fu, Y. Lu, Z. Jiang, R. Chen, Y. Men, Towards a better understanding of the crystallization and melting behaviors of high-density polyethylene samples prepared from quasi-isothermal and stretching oriented localized melts, Polymer 218 (2021) 123485.
[27] R. Seguela, Plasticity of semi-crystalline polymers: crystal slip versus melting-recrystallization, E-Polymers 7 (2007) 382–391.
[28] A. Thévenon, R. Fulchiron, Evolution of poly(propylene) morphology in the rubbery state under uniaxial strain, Macromol. Mater. Eng. 299 (2014) 165–177.
[29] Y. Lu, R. Chen, J. Zhao, Z. Jiang, Y. Men, Stretching temperature dependency of fibrillation process in isotactic polypropylene, J. Phys. Chem. B 121 (2017) 6969–6978.
[30] X. Chen, F. Lv, F. Su, Y. Ji, L. Meng, C. Wan, Y. Lin, X. Li, L. Li, Deformation mechanism of iPP under uniaxial stretching over a wide temperature range: an in-situ synchrotron radiation SAXS/WAXS study, Polymer 118 (2017) 12–21.
[31] F. Auriemma, C. De Rosa, R. Di Girolamo, A. Malafronte, M. Scoti, G.R. Mitchell, S. Esposito, Deformation of stereoirregular isotactic polypropylene across length scales. Influence of temperature, Macromolecules 50 (2017) 2856–2870.
[32] Y. Nie, H. Gao, M. Yu, Z. Hu, G. Reiter, W. Hu, Competition of crystal nucleation to fabricate the oriented semi-crystalline polymers, Polymer 54 (2013) 3402–3407.
[33] B. Chang, H. Shi, M. He, K. Schneider, G. Heinrich, C. Liu, C. Shen, The retardation effects of lamellar slip or/and chain slip on void initiation during uniaxial stretching of oriented iPP, Polymer 215 (2021) 123342.
[34] H. Zhou, G.L. Wilkes, Orientation-dependent mechanical properties and deformation morphologies for uniaxially melt-extruded high-density polyethylene films having an initial stacked lamellar texture, J. Mater. Sci. 33 (1998) 287–303.
[35] G. Fritz-Popovski, M. Feuchter, G.A. Maier, Deformation mechanisms in uniaxial-oriented semi-crystalline PET-films as a function of orientation to tensile direction, J. Polym. Sci. B Polym. Phys. 56 (2018) 159–169.
[36] B. Chang, K. Schneider, F. Xiang, R. Vogel, S. Roth, G. Heinrich, Critical strains for lamellae deformation and cavitation during uniaxial stretching of annealed isotactic polypropylene, Macromolecules 51 (2018) 6276–6290.
[37] The Mechanical Properties of Polymers: General Considerations, Mechanical Properties of Solid Polymers2012, pp. 19-29.
[38] C.R. López-Barrón, Y. Zeng, J.J. Schaefer, A.P.R. Eberle, T.P. Lodge, F.S. Bates, Molecular alignment in polyethylene during cold drawing using in-situ SANS and Raman spectroscopy, Macromolecules (2017).
[39] R. Seguela, On the strain-induced crystalline phase changes in semi-crystalline polymers: mechanisms and incidence on the mechanical properties, J. Macromol. Sci. Polym. Rev. 45 (2005) 263–287.
[40] Y. Chen, S. Yang, H. Yang, G. Zhong, D. Fang, B.S. Hsiao, Z. Li, Deformation behavior of oriented β-crystals in injection-molded isotactic polypropylene by in situ X-ray scattering, Polymer 84 (2016) 254–266.
[41] R.-Y. Bao, Z.-T. Ding, Z.-Y. Liu, W. Yang, B.-H. Xie, M.-B. Yang, Deformation-induced structure evolution of oriented β-polypropylene during uniaxial stretching, Polymer 54 (2013) 1259–1268.
[42] F. Yang, F. Yang, M. Xiang, T. Wu, Preparation of highly oriented β polypropylene and its pore formation mechanism during stretching, Polymer Crystallization, n/a e10183.
[43] B. Chang, K. Schneider, R. Vogel, G. Heinrich, Influence of nucleating agent self-assembly on structural evolution of isotactic polypropylene during uniaxial stretching, Polymer 138 (2018) 329–342.
[44] A.J. Lovinger, J.O. Chua, C.C. Gryte, Studies on the α and β forms of isotactic polypropylene by crystallization in a temperature gradient, J Polym Polym Phys Ed 15 (1977) 641–656.
[45] Y. Chen, B. Xu, H. Yang, Q. Zhang, Z. Li, Deformation behavior of isotactic polypropylene with oriented α- and β-crystals, Mater. Lett. 219 (2018) 209–211.
[46] T. Wu, M. Xiang, Y. Cao, J. Kang, F. Yang, Pore formation mechanism of [small beta] nucleated polypropylene stretched membranes, RSC Adv. 4 (2014) 36689–36701.
[47] K.-H. Nitta, H. Nomura, Stress–strain behavior of cold-drawn isotactic polypropylene subjected to various drawn histories, Polymer 55 (2014) 6614–6622.
[48] Y.-A. Kang, K.-H. Kim, S. Ikehata, Y. Ohkoshi, Y. Gotoh, M. Nagura, H. Urakawa, In-situ analysis of fiber structure development for isotactic polypropylene, Polymer 52 (2011) 2044–2050.

[49] S.A. Jabarin, Strain-induced crystallization of poly(ethylene terephthalate), Polym. Eng. Sci. 32 (1992) 1341–1349.
[50] Y. Mao, D.G. Bucknall, R.M. Kriegel, Synchrotron X-ray scattering study on amorphous poly(ethylene furanoate) under uniaxial deformation, Polymer 139 (2018) 60–67.
[51] E. Forestier, C. Combeaud, N. Guigo, G. Monge, J.-M. Haudin, N. Sbirrazzuoli, N. Billon, Strain-induced crystallization of poly(ethylene 2,5-furandicarboxylate). Mechanical and crystallographic analysis, Polymer 187 (2020) 122126.
[52] G. Stoclet, J.M. Lefebvre, B. Yeniad, G. Gobius du Sart, S. de Vos, On the strain-induced structural evolution of Poly(ethylene-2,5-furanoate) upon uniaxial stretching: an in-situ SAXS-WAXS study, Polymer 134 (2018) 227–241.
[53] E. Forestier, C. Combeaud, N. Guigo, N. Sbirrazzuoli, N. Billon, Understanding of strain-induced crystallization developments scenarios for polyesters: comparison of poly(ethylene furanoate), PEF, and poly(ethylene terephthalate), PET, Polymer 203 (2020) 122755.
[54] J.R. Katz, Röntgenspektrographische Untersuchungen am gedehnten Kautschuk und ihre mögliche Bedeutung für das Problem der Dehnungseigenschaften dieser Substanz, Naturwissenschaften 13 (1925) 410–416.
[55] J. Zhao, P. Chen, Y. Lin, W. Chen, A. Lu, L. Meng, D. Wang, L. Li, Stretch-induced intermediate structures and crystallization of poly(dimethylsiloxane): the effect of filler content, Macromolecules 53 (2020) 719–730.
[56] P. Zhang, G. Huang, L. Qu, Y. Nie, G. Weng, J. Wu, Strain-induced crystallization behavior of polychloroprene rubber, J. Appl. Polym. Sci. 121 (2011) 37–42.
[57] P.-Y. Le Gac, P.-A. Albouy, D. Petermann, Strain-induced crystallization in an unfilled polychloroprene rubber: kinetics and mechanical cycling, Polymer 142 (2018) 209–217.
[58] P.-A. Albouy, G. Guillier, D. Petermann, A. Vieyres, O. Sanseau, P. Sotta, A stroboscopic X-ray apparatus for the study of the kinetics of strain-induced crystallization in natural rubber, Polymer 53 (2012) 3313–3324.
[59] K. Brüning, K. Schneider, S.V. Roth, G. Heinrich, Kinetics of strain-induced crystallization in natural rubber studied by WAXD: dynamic and impact tensile experiments, Macromolecules 45 (2012) 7914–7919.
[60] P.J. Flory, Thermodynamics of crystallization in high polymers. I. crystallization induced by stretching, J. Chem. Phys. 15 (1947) 397–408.
[61] J. Rault, J. Marchal, P. Judeinstein, P.A. Albouy, Chain orientation in natural rubber, Part II: 2H-NMR study, The European Physical Journal E 21 (2006) 243–261.
[62] N. Candau, L. Chazeau, J.-M. Chenal, C. Gauthier, E. Munch, Complex dependence on the elastically active chains density of the strain induced crystallization of vulcanized natural rubbers, from low to high strain rate, Polymer 97 (2016) 158–166.
[63] J.-M. Chenal, L. Chazeau, L. Guy, Y. Bomal, C. Gauthier, Molecular weight between physical entanglements in natural rubber: a critical parameter during strain-induced crystallization, Polymer 48 (2007) 1042–1046.
[64] M. Tosaka, S. Kohjiya, Y. Ikeda, S. Toki, B.S. Hsiao, Molecular orientation and stress relaxation during strain-induced crystallization of vulcanized natural rubber, Polym. J. 42 (2010) 474–481.
[65] S. Toki, T. Fujimaki, M. Okuyama, Strain-induced crystallization of natural rubber as detected real-time by wide-angle X-ray diffraction technique, Polymer 41 (2000) 5423–5429.